4-3 Acoustic Simulation Techniques for Personalized Three-Dimensional Auditory Reproduction

TAKEMOTO Hironori, Parham Mokhtari, NISHIMURA Ryouichi, and KATO Hiroaki

Humans can feel sound three-dimensionally thanks to head-related transfer functions (HRTFs) that result from complex reflection and diffraction by the head and pinna, whose shapes vary greatly among individuals. In three-dimensional auditory reproduction systems, this variation should be considered. To visualize and understand the acoustic phenomena on the head and pinna, we have developed an acoustic simulator based on the finite-difference time-domain method. By using this simulator to clarify the relation between the head/pinna shapes and HRTFs, it is considered possible to elucidate morphological factors providing personal differences in HRTFs. This article first gives an overview of the simulator and its simulation accuracy, and then elucidates the factors regarding the peaks and notches of HRTFs in the median plane based on research results obtained from this simulator.

Keywords
Head-related transfer function, Three-dimensional auditory reproduction, Acoustic simulator, FDTD method

1 Introduction

Various kinds of sound surround us. The sound of rain prompts us to look out the window. When called by someone, we turn around. This is because we have the ability to locate the sound source three-dimensionally. This ability is particularly sharp when the sound source is behind us and compensates for the visual sense.

Sound propagates through the air, gets reflected and diffracted by the head and pinna, passes through the ear canal, and then reaches the eardrum. Of these events, reflection and diffraction by the head and pinna are the most important in locating a sound source in three-dimensional space. Both affect the propagation of sound by intensifying certain frequency bands and weakening other bands. A response which characterizes how each ear receives sounds from a spatial point is called a head-related transfer function (HRTF). Thus, the HRTF varies with the source location and differs between right and left ears which are rarely, if ever, perfectly symmetrical. However, we have learned the patterns of such variations for use in locating sound sources. Moreover, an HRTF for the same source location varies greatly among individuals. This is because patterns of reflection and diffraction change according to different shapes of the head and pinna. Therefore, such differences among individuals must be considered in systems for three-dimensional auditory reproduction.

It is not clear, however, how sound gets reflected and diffracted in the head and pinna. One major impediment is that sound is invisible. Changes in sound pressure at a certain point in space can be measured with a microphone. The number of points that can be measured at the same time is limited, because each

microphone has a certain size and it is difficult to provide and control many microphones with the same characteristics. The required number of microphones can range from dozens to hundreds. Thus, it is difficult to observe reflections and diffractions on the head and pinna, particularly on a small and complex-shaped pinna (see Fig. 1).

We thus developed an acoustic simulator that can visualize temporal changes in the acoustic field. This simulator can import the head and pinna shape measured by magnetic resonance imaging (MRI) as three-dimensional data and calculate changes in sound pressure and particle velocity at all points (tens of millions) at short time intervals. Based on these calculation results, changes in the acoustic field (such as the distribution of pressure) can be visualized using a volume rendering method.

As shown in Fig. 2, we then set up the framework of using computer simulations and acoustic measurements in a mutually complementary manner, thereby allowing us to understand and clarify the complex reflections and diffractions occurring around the head and pinna. By obtaining knowledge about what kind of acoustic phenomenon occurs in which portion of the pinna shape, we could clarify the relation between pinna shape and HRTFs, thereby allowing us to elucidate the morphological factors of personal differences in HRTFs. This article first describes the simulator and its accuracy, and then reports some of our current results concerning how reflections and diffractions on the pinna generate spectral peaks and notches.

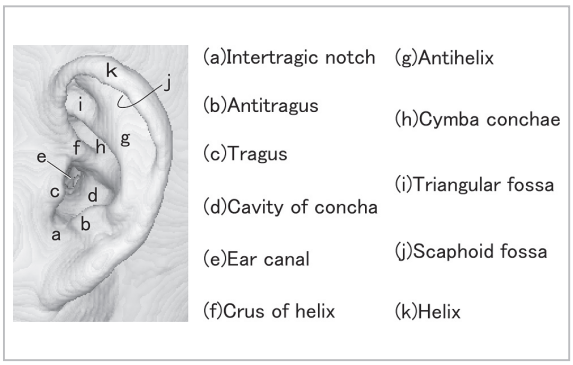

Fig.1 *Shape of the pinna*

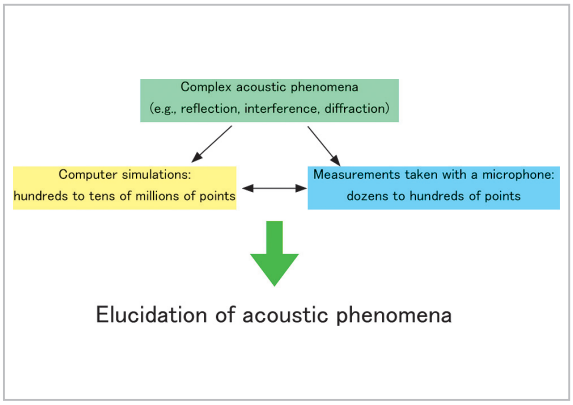

Fig.2 *Research framework*

2 Acoustic simulator

2.1 Finite-Difference Time-Domain (FDTD) method

To simulate changes in sound pressure and particle velocity on the head and pinna in the time domain, we developed an acoustic simulator[3][4] based on the finite-difference time-domain (FDTD) method[1][2]. The FDTD method requires an absorbing boundary around the analysis field to prevent reflection on the outer edges of that field. For this absorbing boundary, we introduced a perfectly matched layer (PML)[5] consisting of eight layers.

The dominant equations for the FDTD method are based on the sound pressure p, particle velocity vector u, sound velocity c, material density ρ, and compressibility of the medium $\kappa = 1/\rho c^2$ as follows:

$$-\kappa\frac{\partial p}{\partial t} - \alpha p = \nabla u\,, \tag{1}$$

$$-\rho\frac{\partial u}{\partial t} - \alpha^* u = \nabla p\,, \tag{2}$$

where, α denotes an attenuation coefficient associated with compressibility of the medium and α^* an attenuation coefficient associated with density of the medium. In PML, $\alpha^* = \alpha\rho/\kappa$. In the analysis region, $\alpha^* = 0$. This was discretized by second-order accurate central difference in

time and fourth-order accurate central difference in space by using the Yee algorithm[6].

The FDTD method can simulate not only stationary phenomena but also transient ones. Moreover, the calculation algorithm is simple and easy to parallelize, and the computational cost is low compared with the finite element method (FEM) and boundary element method (BEM)[7]. In our laboratory, therefore, two computers (each having four CPUs with six cores) are directly connected with each other by InfiniBand to perform parallel calculations by means of the Message Passing Interface (MPI) using a total of 48 cores.

2.2 Verification of accuracy

This section discusses the accuracy of acoustic simulation using the FDTD method. Figure 3 shows the three-dimensional shape of KEMAR (Knowles Electronics Manikin for Acoustic Research)[8], which was measured by Dr. Yuvi Kahana using a laser scanner. KEMAR is a head model widely used in acoustic experiments. Its HRTFs were acoustically measured and publicly distributed in the CIPIC (Center for Image Processing and Integrated Computing, UC Davis) database[9]. We calculated the HRTFs of KEMAR using the scanned head data and FDTD simulation method, and then compared them with the measured HRTFs for verification.

Figure 4 compares calculated HRTFs (blue) of the right ear with measured ones (red) with regard to 45 sound source locations. The azimuth and elevation coordinates are expressed in the inter-aural polar coordinate system whose axis is a straight line going through the right and left ear holes. In terms of azimuth, 0 degrees coincides with the median plane (including the location directly in front), with positive and negative azimuth angles referring

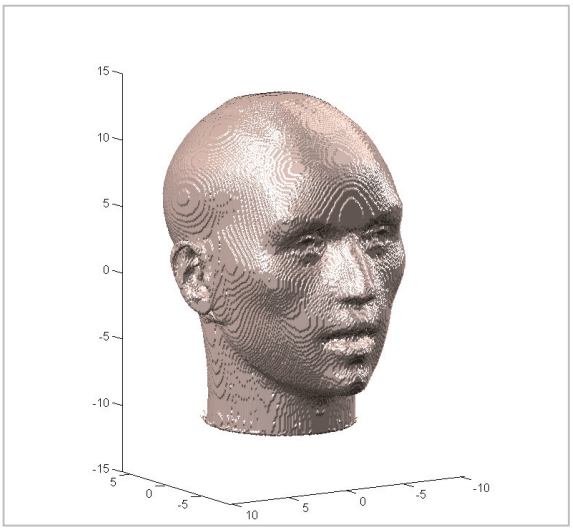

Fig.3 *Shape data of KEMAR*

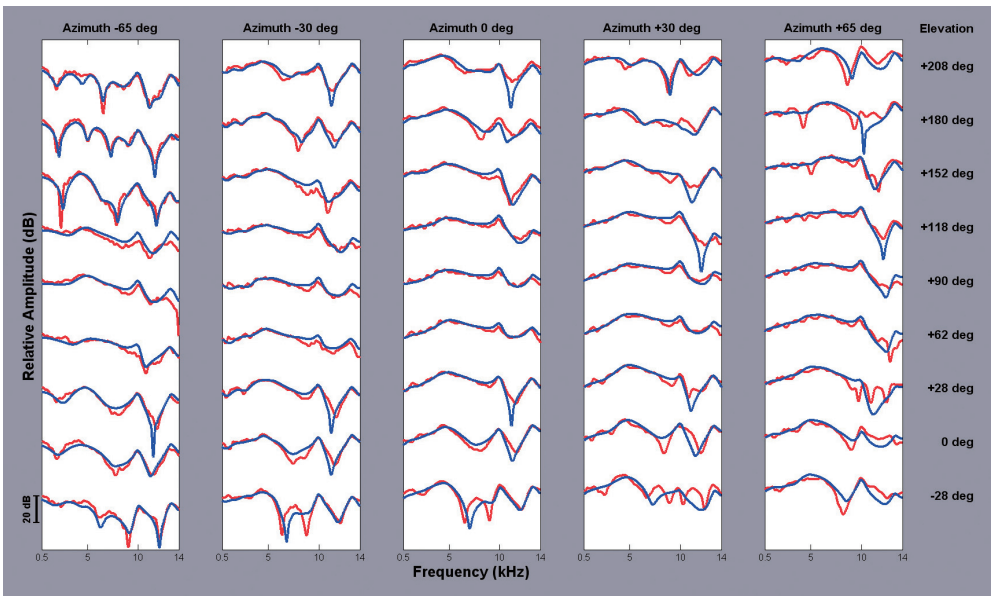

Fig.4 *Calculated HRTFs (blue) and measured HRTFs (red)*

to lateral planes to the right and to the left, respectively. In terms of elevation, 0 degrees refers to the front horizontal plane, 90 degrees is above, and 180 degrees is behind. Calculated HRTFs agreed well with measured ones and the mean spectral distance was 2.3 dB. This KEMAR is bilaterally symmetric, so that HRTFs of the right and left ears should be symmetric with regard to the median plane. However, the mean spectral distance between the measured right- and left-ear HRTFs was 3.1 dB. Although the left and right pinnae used on the physical KEMAR manikin for CIPIC measurements were not perfectly symmetric, this value of 3.1 dB presumably represents mainly measurement errors. Thus, we concluded that FDTD simulations have approximately the same accuracy as acoustic measurements, because the mean spectral distance of 2.3 dB between calculated and measured HRTFs was slightly smaller than the value 3.1 dB probably caused by acoustic measurement errors[10].

3 Example of analysis

This section describes an example of analysis conducted with the acoustic simulator.

3.1 Localizing the elevation angle of a sound source in the median plane

When a sound source is placed within the horizontal plane at a non-zero azimuth angle, the sound wave reaches the near (ipsilateral) ear sooner than the far (contralateral) ear, and the sound intensity is also larger at the near ear. These characteristics can act as important cues for locating the azimuth angle of a sound source on or near the horizontal plane. On the other hand, when a sound source is placed within the median plane, these characteristics don't provide cues for locating the elevation angle, because the distances from the sound source to the right and left ears are approximately the same. Instead, spectral peaks and notches of HRTFs are used as monaural cues for locating the elevation angle.

Figure 5 shows a typical peak-notch pattern of HRTFs in the median plane. The x-axis represents frequency and the y-axis represents elevation angle. Solid lines indicate spectral peaks; dashed lines indicate spectral notches. Below 10 kHz, there are three peaks (P1, P2 and P3) surrounded by two notches (N1 and N2). The peak frequencies are constant, while the peak amplitudes vary with elevation angle so that P2 and P3 appear at a limited range of angles. On the other hand, both the frequency and amplitude of the notches change with elevation angle. The notch frequencies gradually increase from -90 degrees (directly below) to about 120 degrees (30 degrees behind from directly above), and decrease gradually from 120 degrees to 270 degrees elevation. According to perceptual experiments, P1, N1 and N2 are cues for locating the elevation angle of a sound source[11]. Although the typical peak-notch pattern schematized in Fig. 5 is common across individuals, there are individual differences in terms of the amplitudes and frequencies of peaks and notches, the highest notch frequency, and the increasing and decreasing patterns of notches. These facts suggest that the pinna shapes are topologically common among individuals, while partial proportions vary.

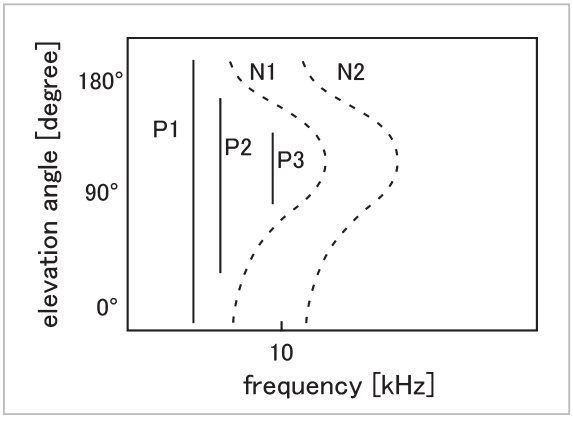

Fig.5 *Typical peak-notch pattern of HRTFs in the median plane*

3.2 Peak-notch pattern of HRTFs in the median plane

It is known that the pinna generates the basic peak-notch patterns of HRTFs in the median plane, while the head affects the pattern mainly on the contralateral side, away from the

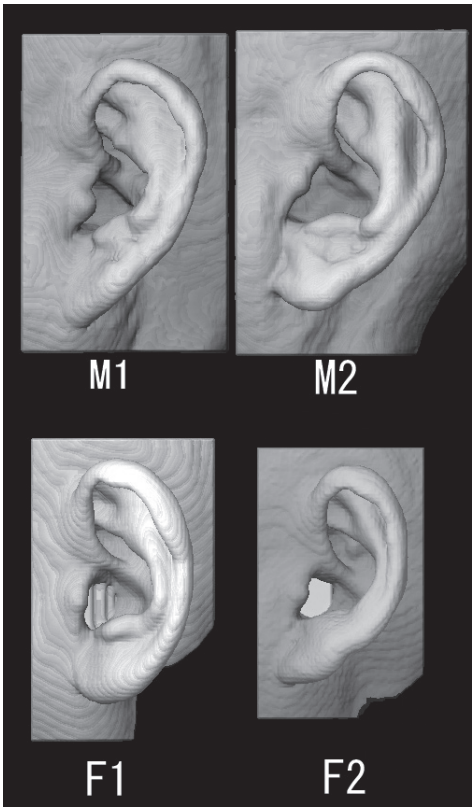

Fig.6 *Pinnae segmented MRI head data for the four subjects*

median plane[10][12]. Figure 6 shows segmented left pinnae from MRI head data for four subjects (males M1 and M2; females F1 and F2). The morphological features of the pinna denoted in Fig. 1 are common among the four subjects. That is, the four pinnae are topologically the same. However, the size of each part (e.g., concha, cymba, triangular fossa, scaphoid fossa) relative to the entire pinna is different for each individual. Figure 7 shows HRTFs in the median plane calculated from the four segmented pinnae using the acoustic simulator. While the typical peak-notch pattern was observed for all four pinnae, the N2 trajectory was not always obvious.

HRTFs were calculated as follows: A sound source point was placed at the entrance of the ear canal, and 36 observation points were placed at 10-degree intervals on a circumference 10 cm in radius within the saggital plane whose center was the source point. A Gaussian pulse was then supplied to the sound source to simulate acoustic propagation. Pressure changes at the observation points were calculated to obtain HRTFs. In a real HRTF measurement, a sound source (loudspeaker) is placed and moved on a circumference, and an observation point (microphone) is fixed at the entrance of the ear canal. That is, the locations of the sound source point and observation point are reverse between measurement and simulation. Due to the reciprocity theorem in acoustics (i.e., the rule of invertibility), however, the pressure changes observed remain constant even when the source point and observation points are changed. Thus, the same HRTF is obtained in both cases.

3.3 Mechanism of peak generation

Shaw's experiments[13][14] and simulations conducted by Kahana et al.[15] using the boundary element method (BEM) have revealed the physical mechanism of the HRTF peaks. That is, among the various resonance modes that occur in the pinna cavities, peaks are those in which a pressure anti-node is generated in the concha. At P1, a single anti-node develops across the pinna cavities including the concha. At P2, one anti-node is generated in the concha and a second one appears in another part. At P3, one anti-node is generated in the concha and two others appear at other parts of the pinna.

In order to confirm these phenomena also in our time-domain simulator, the analysis field was excited at a frequency equal to one of the HRTF peaks by a sinusoidal source, and temporal changes in the pressure distribution pattern on the pinna were visualized by a volume rendering method. In this simulation, the source point at which a sinusoidal wave was fed was placed on the circumference on which the observation points for HRTF calculations were placed. In the visualization, high positive sound pressures are indicated in red, and high negative ones in blue. In other words, a pressure anti-node on the pinna was indicated in red or blue. The red and blue portions, however, are reversed in phase. Moreover, the following figures representing simulation results indicate

one cycle of the excitation wave with four frames of images.

Figure 8 shows changes in the pressure distribution pattern when the pinna of M2 was excited by a sinusoidal wave at P1 frequency (3.5 kHz). The volume of air within all pinna cavities—the concha, cymba, and triangular fossa—became consecutively red then blue, all at the same time. This indicates that all the pinna cavities resonated in phase. Moreover, this is the first resonance mode (1/4 wavelength) when the inward and outward direction of the pinna is assumed to be a pipe closed on one side. Note that although in this figure the sound source was placed at an elevation angle of 0 degrees, the same pressure changing pattern was observed when the sound source was placed at other elevation angles.

Figure 9 shows changes in the pressure distribution pattern when the pinna of M2 was ex-

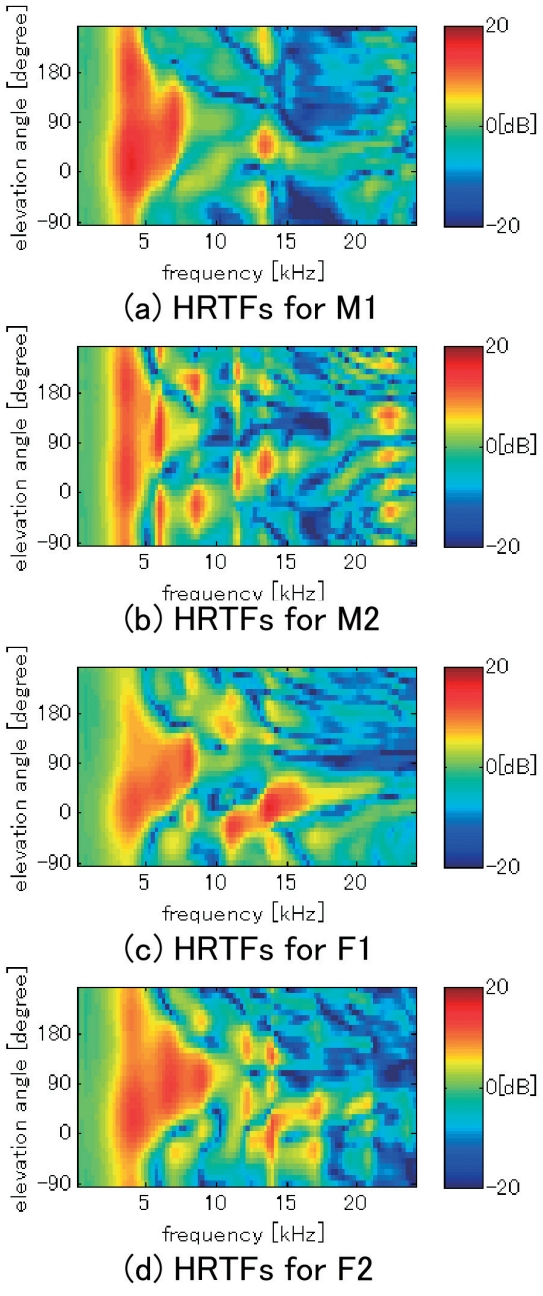

Fig.7 *HRTFs in the median plane for the four subjects*

cited with a sinusoidal wave at P2 frequency (6 kHz). A pressure anti-node appeared in the concha, and another in the portion between the cymba and triangular fossa, along with a reverse phase. This suggests the secondary resonance mode in the pinna cavities. The sound source point at that time was placed at an elevation angle of 60 degrees, but the same resonance mode was observed at any elevation angle where P2 appeared.

Figure 10 shows changes in the pressure distribution pattern when the pinna of M2 was excited with a sinusoidal wave at P3 frequency (8.5 kHz). Pressure anti-nodes appeared in the concha, cymba, and triangular fossa, for a total of three points. The concha and triangular fossa had the same phase, while the cymba had a reverse phase. This suggests that the third resonance mode occurred across these pinna cavities. The sound source point at that time was placed at an elevation angle of 120 degrees, but the same resonance mode occurred at any elevation angle where P3 appeared.

Although the aforementioned results were obtained from M2, the other three subjects showed similar results. As a result, knowledge regarding the physical mechanism of peak generation was confirmed with our simulator.

3.4 Mechanism of notch generation

Although the cancelation between the direct incoming wave and the reflected wave would be a possible hypothesis which accounts for generating notches of HRTFs[16][17], this hypothesis has not been as widely accepted compared with the theory for peaks mentioned above. In particular, it is unknown how the notch is generated when a sound source is placed in the postero-superior direction[17]. We therefore conducted simulations at N1 frequencies corresponding to various elevation angles to visualize and understand how N1 is generated. As a result, we discovered and reported three mechanisms depending on elevation an-

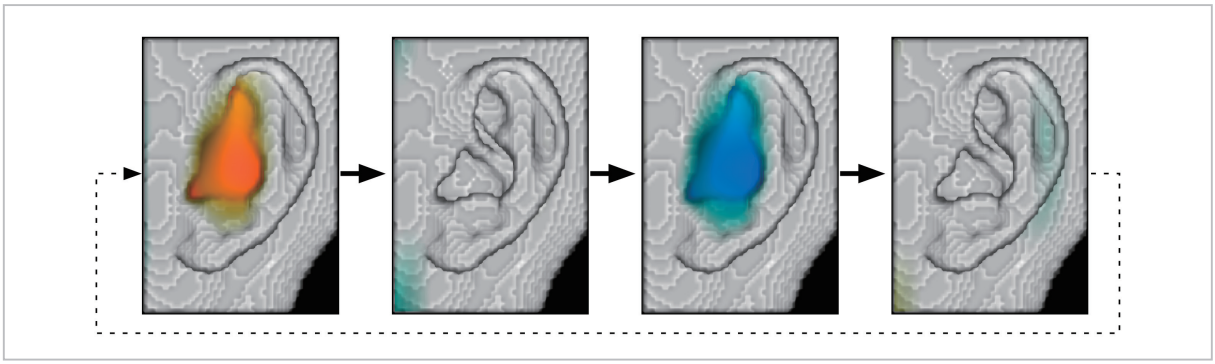

Fig.8 *Changes in pressure distribution pattern at P1 frequency*

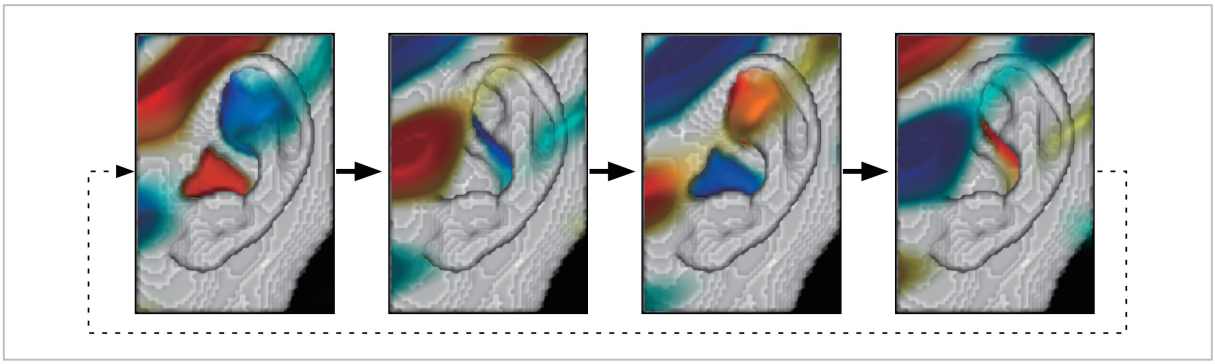

Fig.9 *Changes in pressure distribution pattern at P2 frequency*

gle[18]. This section briefly presents those findings.

First, when the sound source is in a direction less than about 0 degrees or greater than 180 degrees in elevation angle (i.e., below the horizontal plane), N1 is generated under the principle of "counter canceling." In this principle, traveling waves propagated from the sound source are canceled by the resonance of the reverse phase generated in cavities above the concha. Pressure changes, therefore, are minimized in the concha. In other words, a pressure node is generated in the concha.

Figure 11 shows changes in the pressure distribution pattern when simulation was conducted for N1 (5.25 kHz) at an elevation angle of -30 degrees using the pinna of M2. In the first frame, waves traveling from the bottom left to the top right are red. That is, traveling waves have positive sound pressure. Conversely, the cymba, triangular fossa, and scaphoid fossa are blue, indicating that a resonance with reverse phase occurs in these cavities. Therefore, because the traveling waves are canceled by the resonance above the concha, the air within the concha was not colored, indicating very small changes in sound pressure. In the second frame, traveling waves with negative sound pressure come closer from the bottom left. In the third frame, a resonance with positive sound pressure occurs in the cymba, triangular fossa, and scaphoid fossa, as if to defend against the traveling waves. In the fourth frame, traveling waves with positive sound pressure come closer from the bottom left. Then the process returns to the first frame and then the same phenomena are repeated.

Next, when the sound source is placed in the direction between about 0 and 90 degrees (i.e., when ahead and above), then N1 is generated under the principle of "extended counter canceling." This is the extended version of "counter canceling." In addition to the cavity above the concha, the posterior margin of the concha plays a part in canceling the traveling waves. Moreover, in "counter canceling," the

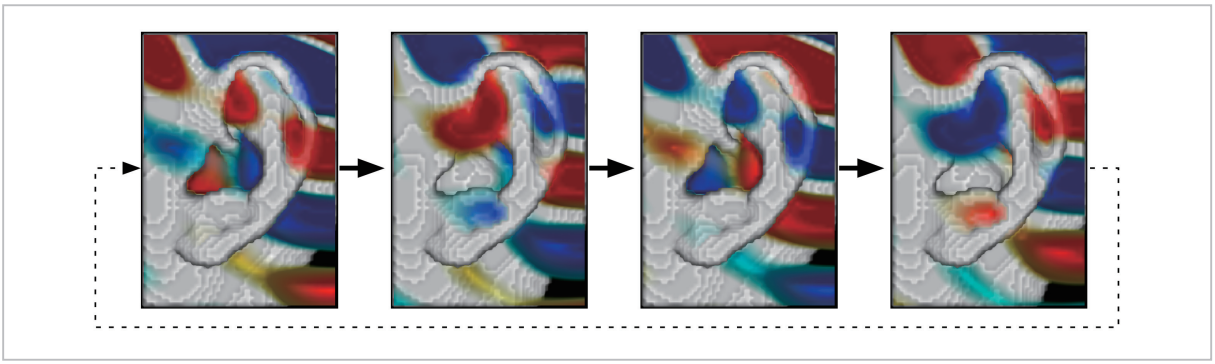

Fig.10 *Changes in pressure distribution pattern at P3 frequency*

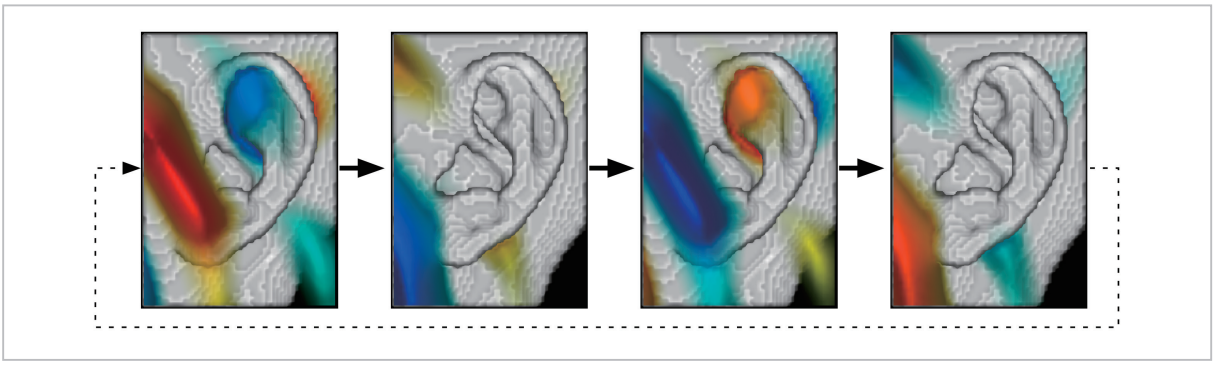

Fig.11 *Mechanism for generating N1: "counter canceling." This type of cancelation is observed when the sound source is placed below the horizontal plane.*

entire cavity above the concha is resonated in phase. On the other hand, in "extended counter canceling," the portion from the cymba to the triangular fossa generates a pressure anti-node of the same phase as that of the traveling waves, while the posterior margin wall of the concha generates a pressure anti-node in reverse phase compared with the traveling waves. Thus, the latter pressure anti-node cancels the traveling waves above the concha.

Figure 12 shows changes in the pressure distribution pattern when the sound source was placed at an elevation angle of 60 degrees and the analysis field was excited at N1 frequency (7.25 kHz) using the pinna of M2. In the first frame, waves with positive sound pressure (red) among the sound waves traveling from the top left to the bottom right have reached the tragus from the triangular fossa. However, the portion from the cymba to the posterior margin of the concha became blue, generating a resonance in reverse phase. This resonance cancels the traveling waves having positive sound pressure, so that pressure changes are minimized in the concha. In the second frame, traveling waves with negative pressure come closer from the top left. In the third frame, sound pressures are arranged in the reverse pattern of the first frame, showing that the traveling waves and posterior margin of the concha cancel each other. In the fourth frame, traveling waves with positive sound pressure come closer from the top left. After that, the process returns to the first frame.

Lastly, when the sound source is placed in the direction between about 90 degrees and 180 degrees in elevation angle, N1 is generated under a principle called "intercept canceling." In this cancelation, a pressure anti-node of the same phase as that of the traveling waves is generated in the triangular fossa, and a pressure anti-node in reverse phase is generated in the cymba. The latter anti-node cancels the traveling waves passing by the outside of the cymba. While the two principles described earlier hold that canceling occurs across the concha, this principle holds that traveling waves passing above the cymba are canceled by the resonance of the cymba from inside the cavity, thereby preventing the waves from reaching the concha (i.e., entrance to the ear canal). In that point, this principle essentially differs from the other two principles.

Figure 13 shows changes in the pressure distribution pattern when the sound source was placed at an elevation angle of 150 degrees and the analysis field was excited at N1 frequency (8.25 kHz) using the pinna of M2. The top row shows a lateral view of the pinna and its pressure distribution pattern; the bottom row shows the cross section and pressure distribution pattern indicated by the yellow dotted line in the top row. In the bottom row, positive high sound pressures are colored in red, negative high sound pressures in blue, and sound pressures close to zero in green. In the first frame, the waves with positive sound pressure coming from the top right reach the region from the triangular fossa to the posterior margin of the concha. At that time, in the cross section shown

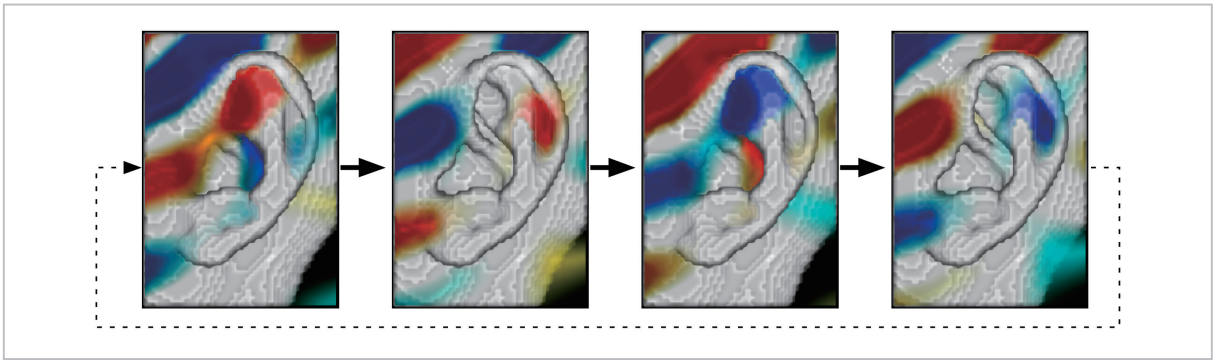

Fig.12 *Mechanism for generating N1: "extended counter canceling." This type of cancelation is observed when the sound source is placed ahead and above.*

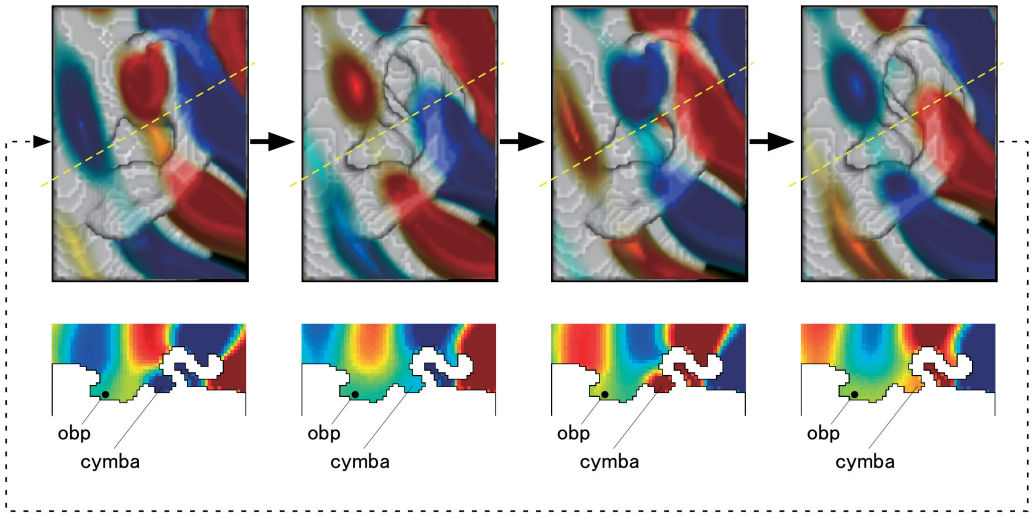

Fig.13 *Mechanism for generating N1 "intercept canceling." This type of cancelation is observed when the sound source is placed behind and above.*

The yellow dotted line in the top row of the diagram indicates the location of the cross section shown in the bottom row.
obp: observation point; cymba: part of the ear

in the bottom row, the cymba (portion marked "cymba") becomes blue and is in reverse phase compared with the sound waves passing by the outside (above in the diagram). Cancellation of the reverse phase between inside and outside the cymba thus reduces changes in sound pressure at the entrance to the ear canal (i.e., at the observation point marked "obp" in the diagram.) In the second frame, the traveling waves with negative sound pressure are about to reach the posterior margin of the concha from the triangular fossa. In the third frame, sound pressures are arranged in reverse polarity compared with the first frame. There again, the sound waves of the reverse phase cancel each other between inside and outside the cymba. In the fourth frame, traveling waves with positive sound pressure come from the top right. After that, the process returns to the first frame and then the same phenomena are repeated.

The point common to all three mechanisms for generating N1 is that the upper cavities above the concha (including the cymba, triangular fossa and scaphoid fossa) resonate in reverse phase compared with the traveling waves, thereby canceling the waves. These observations were only made possible by simulating and visualizing sound propagation in the time domain.

The three mechanisms for generating N1 were also common among the four subjects. This would derive from the fact that, as shown in Fig. 6, the pinna shapes of the four subjects are topologically the same. On the other hand, the difference in N1 frequency and amplitude at the same elevation angle, and the difference in elevation angle at which N1 frequency peaks would be caused by individual differences in pinna shape.

4 Conclusion

This paper first gave an overview of the acoustic simulator and the FDTD method—the simulator's principle of calculation. It then reported that the acoustic simulator proved to have accuracy similar to that of measurements taken with a microphone, based on our verification of accuracy. Finally, the paper described the physical mechanisms of HRTF peaks and

notches in the median plane, as the research results obtained with this simulator.

The research results presented in this paper are acoustic phenomena derived from a topologically common pinna shape. In other words, since the proportions of the pinna do not affect the principles of generating HRTF peaks and notches, it can be called a common feature independent of individuals. However, these proportions do affect the frequency and amplitude of those peaks and notches at the same elevation angle. Therefore, studies are under way concerning the distribution of the pinna's acoustic sensitivity, specifically addressing how these peaks and notches are affected by finely deformed parts of the pinna. We believe that these studies will be able to clarify the factors regarding the personal differences in HRTFs. By promoting such studies, we wish to elucidate more comprehensively the mechanism that allows humans to perceive sound three-dimensionally, and to reproduce 3D audio that matches the head and pinna morphology of each individual, thereby realizing ultra-realism.

Acknowledgments

We wish to thank Dr. Yuvi Kahana for providing us with shape data of KEMAR. Some results presented in this paper were obtained from our collaborative project with Prof. Kazuhiro Iida of Chiba Institute of Technology.

References

1 Yuan, X. and Berggren, M., "Formulation and validation of Berenger's PML absorbing boundary for the FDTD simulation of acoustic scattering," IEEE Trans. Ultrason. Ferroelectr. Freq. Control. 44, 816–822, 1997.

2 Yokota, T., Sakamoto, S., and Tachibana, H., "Visualization of sound propagation and scattering in rooms," Acoust. Sci. & Tech. 23, 40–46, 2002.

3 Takemoto, T., and Mokhtari, P., "Acoustic analysis of the vocal tract by finite difference time domain method," in Proceedings of the Autumn-2007 Meeting of the Acoustical Society of Japan, Kofu, Japan, Paper 1-8-12, pp.475–478, 2007.

4 Mokhtari, P., Takemoto, H., Nishimura, R., and Kato, H., "Efficient computation of HRTFs at any distance by FDTD simulation with near to far field transformation," in Proceedings of the Autumn-2008 Meeting of the Acoustical Society of Japan, Fukuoka, Japan, Paper 1-8-12, pp. 611–614, 2008.

5 Berenger, J. P., "A perfectly matched layer for the absorption of electromagnetic waves," J. Comput. Phys.114, 185–200, 1994.

6 Yee, K. S., "Numerical solution of initial boundary value problems involving Maxwell's equations in isotropic media," IEEE Trans. Antenas Propagat. AP-14, 302–307, 1966.

7 Chiba, O., Kashiwa, T., Shimoda, H., Kagami, S., and Fukai, I., "Analysis of sound fields in three dimensional space by the time-dependent finite-difference method based on the leap frog algorithm," J. Acoust. Soc. Jpn. (J), 49, pp. 551–562, 1993.

8 Burkhard, M. D. and Sachs R. M., "Anthropometric manikin for acoustic research," J. Acoust. Soc. Am. 58, 214–222, 1975.

9 Algazi, V. R., Duda, R. O., Thompson, D. M., and Avendano, C., "The CIPIC HRTF database,"IEEE Workshop on Applic. of Sig. Process. to Audio and Acoustics, 99–102, 2001.

10 Mokhtari, P., Takemoto, H., Nishimura, R., and Kato, H., "Computer simulation of KEMAR's headrelated transfer functions : verification with measurements and acoustic effects of modifying head shape and pinna concavity," in Principles and Applications of Spatial Hearing, World Scientific, 205–215, 2011.

11 Iida, K., Itho, M., Itagaki, A., and Morimoto, M., "Median plane localization using a parametric model of the head-related transfer function based on spectral cues," Appl. Acoust. 68, 835–850, 2007.
12 Takemoto, H., Mokhtari, P., Kato, H., Nishimura, R., and Iida, K., "Effects of individual difference of head shape on head related transfer functions," in Proceedings of the Autumn-2009 Meeting of the Acoustical Society of Japan, Koriyama, Japan, Paper 1-8-12, pp. 475–478, 2007.
13 Shaw, E. A. G., "The external ear : new knowledge in earmolds and associated problems," in : S. C. Dalsgaard (Ed.), Proceedings of the Seventh Danavox Symposium, Scandinavian Audiology, Suppl.5, 24–50, 1975.
14 Shaw, E. A. G., "Acoustical features of the human external ear," in : R. H. Gilkey, T. R. Anderson(Eds.), Binaural and Spatial Hearing in Real and Virtual Environments, Lawrence Erlbaum Associates, Mahwah, NJ, 25–47, 1997.
15 Kahana, Y. and Nelson, P. A., "Boundary element simulations of the transfer function of human heads and baffled pinnae using accurate geometric models," J. Sound and Vibration 300, 552–579, 2007.
16 Hebrank, J. and Wright, D., "Spectral cues used in the localization of sound sources on the median plane," J. Acoust. Soc. Am., 56, 1829–1834, 1974.
17 Raykar, V. C., Duraiswami, R., and Yegnanarayana, B., "Extracting the frequencies of the pinna spectral notches in measured head related impulse responses," J. Acoust. Soc. Am. 118, 364–374, 2005.
18 Takemoto, H., Mokhtari, P., Kato, H., Nishimura, R., and Iida, K., "Pressure distribution patterns on the pinna at spectral peak and notch frequencies of head-related transfer functions in the median plane," in Principles and Applications of Spatial Hearing, World Scientific, 179-194, 2011.

(Accepted Sept. 9, 2010)

TAKEMOTO Hironori, *Ph.D.*
Expert Researcher, Multimodal Communication Group, Universal Media Research Center
Acoustic Engineering

Parham Mokhtari, *Ph.D.*
Expert Researcher, Multimodal Communication Group, Universal Media Research Center
Acoustic Engineering

NISHIMURA Ryouichi, *Ph.D.*
Expert Researcher, Multimodal Communication Group, Universal Media Research Center
Acoustic Engineering

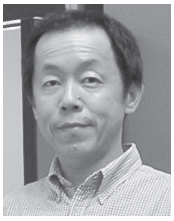

KATO Hiroaki, *Ph.D.*
Research Expert, Multimodal Communication Group, Universal Media Research Center
Acoustic Engineering